Mon. Not. R. Astron. Soc. **266,** 137–154 (1994)

Spectroscopy of A0620 − 00: the mass of the black hole and an image of its accretion disc

T. R. Marsh,[1] E. L. Robinson[2] and J. H. Wood[3]

[1] *University of Oxford, Department of Physics, Nuclear Physics Laboratory, Keble Road, Oxford OX1 3RH*
[2] *University of Texas, Department of Astronomy, Austin, TX 78712, USA*
[3] *Keele University, Department of Physics, Keele ST5 5BG*

Accepted 1993 July 15. Received 1993 July 13; in original form 1993 April 30

ABSTRACT

We present spectra of the black hole binary A0620 − 00 taken at Hα and Hβ to study the distribution of emission-line flux from its accretion disc. Using the spectra of Hα, we have measured the K-type companion star's radial velocity semi-amplitude and rotational broadening to be $K_2 = 433 \pm 3$ km s^{-1} and $v \sin i = 83 \pm 5$ km s^{-1}. Accounting for the Roche-lobe geometry of the companion, the rotational broadening gives the mass ratio $q = M_2/M_1 = 0.067 \pm 0.01$. The disc contributes 6 ± 3 per cent of the light at Hα and 17 ± 3 per cent at Hβ, with the K star providing the rest. The masses of the compact object and K star derived from our values of K_2 and q are $M_1 = (3.09 \pm 0.09) \sin^{-3} i$ M$_\odot$ and $M_2 = (0.21 \pm 0.04) \sin^{-3} i$ M$_\odot$. Applying a constraint upon the orbital inclination, i, from an eclipse found in an earlier study, we obtain 2σ ranges on the masses of $3.30 < M_1 < 4.24$ M$_\odot$ and $0.15 < M_2 < 0.38$ M$_\odot$. The lower limit on the mass of the compact object is higher than the maximum mass of a rotating neutron star based upon equations of state for nuclear material.

Subtraction of the correctly broadened template star removes all lines other than a line at 6708 Å which we identify as Li I 6707.8 Å, which has recently been found in another black hole binary, V404 Cyg. The equivalent width of this line in A0620 − 00 is 160 ± 30 mÅ compared to 290 ± 50 mÅ in V404 Cyg.

Doppler images of the Balmer lines are very similar to those of quiescent dwarf novae, with emission from the region where the gas stream hits the disc and emission from the stream itself prior to this point. The Balmer decrement steepens towards the outer edge of the disc. The impact point gives a disc radius of $\approx 0.5\,R_{L1}$, where R_{L1} is the inner Lagrangian point distance, consistent with the separation of the emission-line peaks. In general, the spectra appear to be of lower excitation than those of dwarf novae, with no He II 4686 emission, weak He I emission and Balmer emission of large equivalent width. There is thus very little ionizing radiation in the system, and a rough analysis suggests that the accretion rate on to the compact object must be less than about 4×10^{12} g s^{-1}.

Key words: accretion, accretion discs – black hole physics – binaries: close – stars: individual: A0620 − 00 – stars: rotation –X-rays: stars.

1 INTRODUCTION

A0620 − 00 (≡V616 Mon) was discovered as a soft X-ray transient in 1975 (Elvis et al. 1975). Subsequent observations revealed that A0620 − 00 is a binary star with an orbital period of 7.75 h, and that the companion to the X-ray source is a K dwarf (Oke 1977; McClintock et al. 1983). Since the outburst, the K star has come to dominate the optical spectrum, and McClintock & Remillard (1986, hereafter MR) were thus able to measure its radial velocity variations. They found a semi-amplitude of 457 km s^{-1}, giving a minimum mass for the compact object of 3.8 M$_\odot$ and immediately placing A0620 − 00 amongst the best black hole candidates. Since MR's discovery, the compact objects in several more X-ray transients have been found to have large masses (V404 Cyg – Casares, Charles & Naylor 1992; X-ray

nova Muscae – Remillard, McClintock & Bailyn 1992), suggesting that we may at last have a reliable indicator of the presence of black holes in binaries.

Haswell & Shafter (1990) detected radial velocity variations of the emission lines which come from an accretion disc surrounding the compact object. They deduced the mass ratio from the amplitude of these variations, but the phase was offset from the expected antiphasing with respect to the red star, indicating that the emission lines were distorted by asymmetries in the disc. An earlier study by Johnston, Kulkarni & Oke (1989) also revealed such asymmetries, but apparently unusually placed in comparison to asymmetries in cataclysmic variable stars. They deduced an extreme mass ratio $q < 0.01$, and showed that the disc must also fill the compact star's Roche lobe. Haswell et al. (1993) found an eclipse of the K star by the disc, and again deduced a large radius for the disc. These results contrast with cataclysmic variable stars, in which the discs typically extend out to only 50 or 60 per cent of the inner Lagrangian point distance.

In order to clarify the nature of the emission from the disc, we obtained spectra of A0620 − 00 with higher spectral resolution and signal-to-noise ratios than the earlier studies. We find that the disc in A0620 − 00 is very similar to those of dwarf novae. As by-products, we have detected Li I 6708 in the atmosphere of the K star, and we have determined the mass ratio of the binary independently of the emission-line radial velocities. We begin with a description of the observations.

2 OBSERVATIONS AND THEIR REDUCTION

The spectra were taken at the Cassegrain focus of the 4.2-m William Herschel Telescope (WHT) with the double-beam spectrograph ISIS on 1991 December 31 and 1992 January 1. We took 51 spectra on the red arm of ISIS, and 11 on the less-sensitive blue arm, with full width half maximum (FWHM) resolutions of 1.5 Å on each arm. Further details are contained in Table 1. The seeing on the first night was typically between 2.5 and 3 arcsec, but had improved to about 1.5 to 2 arcsec on the following night. The poor seeing of the first night meant that our data were readout-noise-limited, and therefore for the second night we binned the CCD pixels on readout into groups of three along the slit. This was effective in reducing the readout noise, and so the second night's data are of higher signal-to-noise ratio than the first. The effect was particularly apparent in the blue spectra, which are as a consequence all from the second night. We observed with a slit width of 1 arcsec throughout in order to obtain accurate radial velocities.

Spectra of comparison arc lamps were taken every fourth exposure on the red arm, and every other exposure on the blue arm. Some cloud was present on each night, and so we could not obtain an absolute flux calibration. Nevertheless, we took wide-slit spectra of the flux standard HD 19445 (Oke & Gunn 1983) on each night for relative flux calibration. We observed BS 753, variously listed as a K3 or K4 dwarf, which we use for cross-correlation in the next section. We took care to observe this star through a slit of the same width as used for A0620 − 00.

Table 1. Journal of observations.

	Red arm	Blue arm
Detector	1280 × 1180 EEV CCD	1280 × 1180 EEV CCD
Wavelength range	5870 – 6780 Å	4380 – 5270 Å
FWHM resolution	1.5Å ≡ 70 km s^{-1}	1.5Å ≡ 90 km s^{-1}
Exposure times	600 s	1920 s
Number of spectra	18 night 1, 33 night 2	11 night 2

The Cassegrain rotator failed shortly before our run, and we were therefore unable to position our long slit to include another star. Since the WHT is mounted on altitude/azimuth axes, the angle of the slit rotates relative to the star field during tracking. Therefore we had to select regions for the estimation of the sky background separately for each exposure. Once the regions were selected, the sky background under the target was interpolated with linear fits for each row of the CCD. We then extracted the spectra, weighting to obtain the maximum signal-to-noise ratio (Horne 1986).

The comparison arc spectra were extracted with the same weights and at the same positions as the target, and fitted with third-order polynomials for both blue and red arms. The rms scatters of the fits for each arm were of order 1/20th of a pixel. With four coefficients fitted to about 30 lines in each case, the statistical uncertainty in the wavelength scale is therefore of order $1/20\sqrt{30/4} \approx 1/50$th of a pixel. This corresponds to 0.9 and 0.7 km s^{-1} for the blue and red arms of the spectrograph, respectively.

3 RESULTS

3.1 Radial velocity of the secondary star

Our first task was to measure the radial velocity of the K-type secondary star in order to subtract its spectrum and to obtain an accurate orbital phase. The radial velocities were measured from the red spectra by cross-correlation (Tonry & Davis 1979) with our template star. Prior to cross-correlating, the spectra were interpolated on to a logarithmic wavelength scale, and a bandpass filter was applied to reduce power outside the range 30 to 300 cycle spectrum^{-1}. This removes low frequencies which may be corrupted by spurious variations in the continuum, and high frequencies which are dominated by noise. We also masked regions near night-sky lines (which included the sodium D lines), an interstellar feature at 6280 Å, Hα and He I 6678 before correlating the spectra. We carried out this analysis twice; the results of the first analysis allowed us to measure a rough value for the rotational broadening of $v \sin i = 80$ km s^{-1} (a more accurate value is derived in the next section), and therefore we repeated the cross-correlation after broadening the template star by this amount in order to simulate the spectrum of the secondary star in A0620 − 00 more accurately. We refined the position of the cross-correlation maximum by parabolic interpolation of three values near the peak, and estimated the uncertainty in this position by propagation of statistical uncertainties. No attempt was made to account for systematic errors caused by, for example, template mismatch. Judging from the χ^2 per degree of freedom of the orbital fit (≈ 1.3), our purely statistical estimates are close to the truth.

The velocities of 48 spectra are plotted in Fig. 1; three spectra were too noisy to obtain a reliable peak, and were not used for the fit. After adding the radial velocity of our standard ($+23$ km s^{-1}), our best fit to the heliocentric radial velocities is

$$V = (4.0 \pm 2) + (432.8 \pm 3) \sin 2\pi[\phi - (5.7 \pm 1) \times 10^{-3}] \text{ km s}^{-1},$$

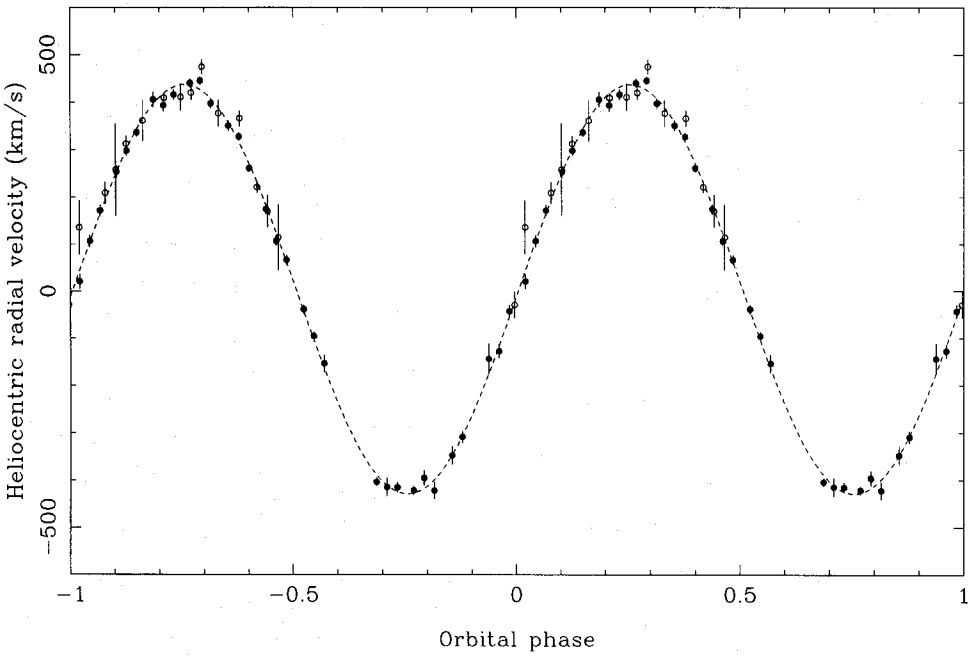

Figure 1. The radial velocities and a circular orbit fit are plotted versus phases derived from McClintock & Remillard's (1986) ephemeris. Open circles are from the first night, and filled circles are from the second night. The data have been plotted twice over two cycles.

where the phases were measured relative to the ephemeris of MR. The uncertainties are 1σ single-parameter estimates based on a bootstrap analysis (Marsh 1988). The uncertainty in our phase is such that the Doppler images to be presented later are correct in angle to within 0°.4. MR's ephemeris, extrapolated to the epoch of our observations, is uncertain by 0.1 cycle, and thus the close agreement of our conjunction phase with the value predicted from their ephemeris appears to be fortuitous. In the rest of this paper, we use phases based upon the conjunction phase of the above fit.

The absorption-line radial velocity semi-amplitude we have obtained, $K_{\rm abs}=433\pm3$ km s^{-1}, should be compared to the results of MR, Johnston et al. (1989), Johnston & Kulkarni (1990) and McClintock & Remillard (1989), who obtained $K_{\rm abs}=457\pm8$, 462 ± 44, 453 ± 11 and 442 ± 4 km s^{-1}, respectively. The difference between our result and that of MR is significant at the 3σ level, and is reminiscent of the real variations in absorption-line radial velocities observed in SS Cyg (Robinson & Zhang 1986). In this case, however, we believe that the uncertainty on MR's result has been underestimated as a result of a subtle problem with their analysis, which we discuss briefly in the following paragraph and more fully in the appendix. The value they obtained on their first fit, $K=444\pm60$ km s^{-1}, is not affected by this problem and is consistent with ours. Consequently, none of the differences in the published K velocities is significant.

MR first obtained velocities based on cross-correlation with a standard-star template. They then shifted out the velocities of this first fit from their spectra, averaged the result, and used this as a new template on the basis that it does not suffer from the spectral type mismatch problems which they believed dominated their uncertainties in the first fit. The uncertainties were indeed greatly reduced; however, we believe that the cross-correlations with the standard star were, in fact, dominated by statistical noise, and that the subsequent improvement was spurious. This can best be appreciated from our improved radial velocities from correlation with a standard star. If MR's hypothesis is correct, this can only have come about through a better spectral-type match; however, MR employed a greater range of spectral types than us, and so we reject this possibility. Instead, the improvement has come about through higher signal-to-noise ratios in our spectra. Johnston et al. (1989) have made the same point, and found no improvement when using a shifted template.

We believe that the cause of the problem is that with the composite template any noise on the component spectra is now present in the template as well. It is then possible for a spurious correlation to be introduced which leads one to underestimate the uncertainties. The analysis of this effect may be of interest to those who use cross-correlation, but would be a diversion from the track of this paper, and therefore we leave it to the appendix.

The radial velocity semi-amplitude is the first step in subtracting the K star from the spectra. We also need to estimate how much the lines are broadened by the rapid rotation of the secondary star, and what fraction of the continuum comes from this star. Not only is the value of the rotational broadening needed for an accurate subtraction of the template, but it also constrains the mass ratio of the binary.

3.2 The rotational broadening and binary mass ratio

We estimated the rotational broadening and the fraction of the flux contributed by the disc by shifting each spectrum by an amount computed from the fit of the previous section, and averaging the results to obtain the mean spectrum of A0620−00 in the rest frame of the secondary star. We then subtracted a constant, representing the fraction of flux from

the K star, times a rotationally broadened version of the template. Next, we applied a high-pass filter to the difference spectrum to remove any large-scale spectral features caused by, for example, the disc continuum, and then computed the χ^2 of the result in regions containing strong K-star absorption lines. The minimum value of χ^2 and its behaviour near the minimum were used to derive the parameters of interest and their uncertainties. Prior to subtraction the A0620−00 spectrum was dereddened, assuming $E(B-V)=0.39$ (Wu et al. 1976), and both the A0620−00 and template spectra were normalized in exactly the same regions, avoiding Hα and strong sky lines (including the sodium D absorption lines which were affected by street lights).

This procedure is complicated by several effects. The rotational broadening that we find, $v \sin i = 83$ km s^{-1}, is small compared to the radial velocity amplitude, and thus the K-star lines can move by an amount comparable to their width during relatively short fractions of an orbit. This motion smears the lines by as much as $2\pi KT/P$ km s^{-1}, where T is the exposure time, and P is the orbital period (the effect is maximal at the conjunction phases). On the red arm $T=600$ s, which gives a maximum shift of ≈ 60 km s^{-1}, and on the blue arm $T=1920$ s, which gives a maximum of ≈ 190 km s^{-1}. Another effect that we shall include below is the non-spherical shape of the secondary star which fills its Roche lobe, but first we deal with the orbital smearing.

We simulated the effect of the orbital motion by smearing the template star by the shift in velocity suffered by each A0620−00 spectrum, which we computed from our radial velocity fit. The 51 smeared spectra were then averaged with the same weights as those used to average the A0620−00 spectra (the weights were chosen to maximize the signal-to-noise ratio of the average). The average smeared spectrum was then broadened and subtracted as described above, and we found $v \sin i = 83 \pm 5$ km s^{-1}, and that the K star contributes 94 ± 4 per cent of the continuum near Hα. (The operations of broadening and smearing are commutative, but fewer computations are required if the smearing is carried out first.) A linear limb-darkening coefficient $\varepsilon = 0.65$ was assumed in deriving the rotational broadening, based on the work of Al-Naimiy (1978) and Wade & Rucinski (1985).

The rotational broadening is related to the radial velocity semi-amplitude and the mass ratio. For the low mass ratio of A0620−00, we can use Paczyński's (1971) formula for the radius of the secondary's Roche lobe, and we find

$$\frac{v \sin i}{K_2} = 0.46[(1+q)^2 q]^{1/3},$$

where K_2 is the radial velocity semi-amplitude of the secondary star. The formula also shows that the fractional error in q for $q \ll 1$ is about three times that in $v \sin i/K_2$, and thus we obtain $q = 0.064 \pm 0.01$.

Armed with this preliminary value of q, we are at last in a position to account for the shape of the Roche lobe which has so far been taken to be spherical. We have done so with model profiles for every observed phase, computed by integrating over a grid on the surface of the Roche lobe, accounting for the orientations and areas of the surface elements in the same manner as Marsh (1988) and Wade & Horne (1988). We included orbital smearing, by computing seven profiles across each phase bin and averaging the result. These profiles were then used to broaden the template 51 times, and then averaged to form an accurately broadened template. This procedure was carried out for models with mass ratios ranging from 0.05 to 0.10, inclination angles of 40°, 55° and 70°, and two values of limb darkening differing by 10 per cent. We used a quadratic limb-darkening law from Wade & Rucinski (1985) for the models with the specific intensity given as a function of $\mu = \cos\theta$ by $I \propto 1 - a(1-\mu) - b(1-\mu)^2$. Values of a and b were taken for $\log g = 4.5$, $T = 5500$ K from Wade & Rucinski (1985), and then scaled to $T = 4500$ K from the linear coefficients of Al-Naimiy (1978).

Gravity darkening was approximated by $T_{\rm eff} \propto g^{\beta}$, with the gravity g calculated from the gradient in the Roche potential for every grid element. For radiative stars $\beta = 0.25$, but it is lower for convective stars. We take $\beta = 0.08$ (Lucy 1967; Sarna 1989). Anderson & Shu (1977) argue for a still lower value of $\beta \approx 0$, and Sarna (1989) finds that somewhat lower values ($\beta = 0.05$) may be more appropriate for cataclysmic variable stars. We therefore computed one model with $\beta = 0$ to judge the effect of this uncertainty. The gravity darkening was included only in as much as it reduces the flux from an element; no account was taken of its possible effect upon the equivalent widths of the lines.

The best-fitting values of the mass ratio, q, and the fraction of the template subtracted, f, are listed as functions of the inclination and limb darkening in Table 2. The best-fitting value (for $i = 70°$) of $q = 0.067 \pm 0.01$ differs little from the approximate estimate from before. The uncertainties quoted on q and f were estimated by changing each parameter from its best-fitting value, and re-minimizing χ^2. The uncertainty was then taken to be the change needed to force the minimum χ^2 to increase by one. These are single-parameter estimates, but f and q are also positively correlated, with a correlation coefficient $r = 0.74$, because a larger q

Table 2. Fits to the rotational broadening.

Inclination	Limb darkening		Gravity	Mass ratio	Fraction of	Minimum
	Lin.	Quad.	Dark.		K star	χ^2
40°	0.60	0.20	0.08	0.0667 ± 0.01	0.939 ± 0.04	641.0
55°	0.60	0.20	0.08	0.0670 ± 0.01	0.939 ± 0.04	641.0
70°	0.60	0.20	0.08	0.0671 ± 0.01	0.939 ± 0.04	641.1
70°	0.60	0.20	0.00	0.0617 ± 0.01	0.939 ± 0.04	640.9
70°	0.66	0.22	0.08	0.0699 ± 0.01	0.939 ± 0.04	641.1

Note: the number of degrees of freedom was 673.

produces broader lines, and thus f must be increased to obtain the best fit.

We list results in Table 2 with sufficient accuracy for the trends with orbital inclination and with limb and gravity darkening to be noticeable. As expected, the variation with inclination is very small, and certainly negligible compared to the statistical uncertainty. Limb and gravity darkening both make the star appear smaller, and lead to increased mass ratios. The limb darkening that we have used is that appropriate to the continuum and may not apply to the lines. Since the lines are formed higher in the atmosphere, we expect the line-centre flux to decrease more slowly as the limb of the star is approached than does the continuum. We therefore anticipate that the equivalent widths might decrease towards the limb, effectively increasing the limb darkening. This would cause us to underestimate q, but a full model-atmosphere calculation for our specific wavelength region is needed to test this. Uncertainties in the gravity and limb darkenings are probably the chief source of systematic error, but it seems likely that statistical uncertainty is dominant.

We did not try to derive independently the mass ratio from the blue data, because the smearing is three times larger and the data are of lower signal-to-noise ratio. Instead, we took the value of $q=0.067$ derived from the red data, computed profiles appropriate to the phases of the blue spectra, and then computed the optimum scale factor for subtraction. The K star contributes 83 ± 4 per cent of the continuum in the blue spectra. This should be compared to 94 ± 3 per cent for the red side (the slightly smaller error compared to that quoted in Table 2 comes from taking a fixed $q=0.067$). These figures suggest that the continuum from the disc is bluer than the K star, as might be expected. However, the contribution from the disc is small in each wavelength range, and suffers a large percentage error as a result.

3.3 The spectra with the secondary star spectrum subtracted

We used the best-fitting model for $i=70°$ (there is virtually no difference for other i) from the previous section to remove the spectrum of the secondary star from the A0620−00 spectra. We present the result in two ways. Figs 2 and 3 show the red and blue spectra shifted into the rest frame of the secondary star, along with the broadened template and the difference between the two. As found already by MR, many K-star features are obvious in the spectrum of A0620−00, and they are almost all removed on subtraction. The Na D lines were not used to estimate the best fit as they are affected by night-sky emission, but even they are removed well. The rise in the spectrum in their vicinity in the difference spectrum is probably He I 5876 emission. Weak He I 6678 emission is visible to the red of Hα. The only features to remain are a broad absorption at 6280 Å, which is a Doppler-smeared interstellar line, and a line on the red side of He I 6678. The latter has a wavelength in the rest frame of the secondary star of 6708.24 ± 0.25 Å, where the wavelength was measured by maximizing the cross-correlation with a Gaussian of FWHM 100 km s^{-1}, with uncertainties on the spectrum propagated through to give the quoted uncertainty. We identify this as Li I 6707.84 from the K star, which was recently found in another black hole candidate, V404 Cyg (Martin et al. 1992; Wallerstein 1992).

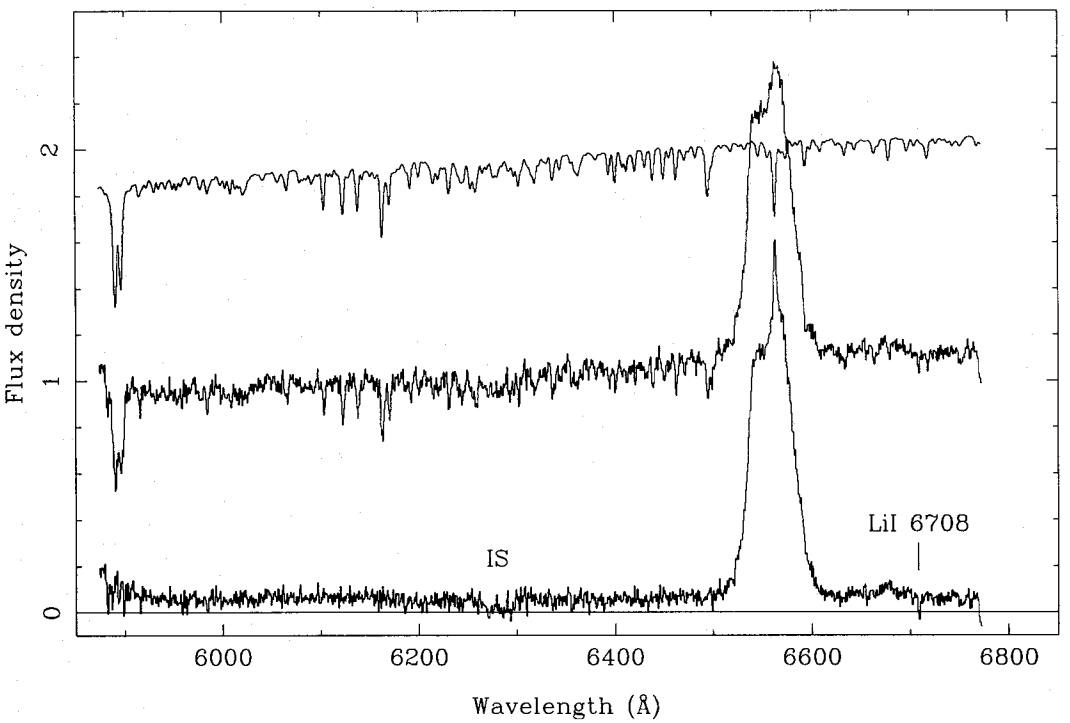

Figure 2. The average spectrum of A0620−00 in the rest frame of the secondary star is plotted (centre spectrum) along with the template spectrum at the top, broadened to match A0620−00. The difference between these is plotted at the bottom. All lines of the K star are removed, except for a line at 6708 Å, which we identify as Li I 6708.

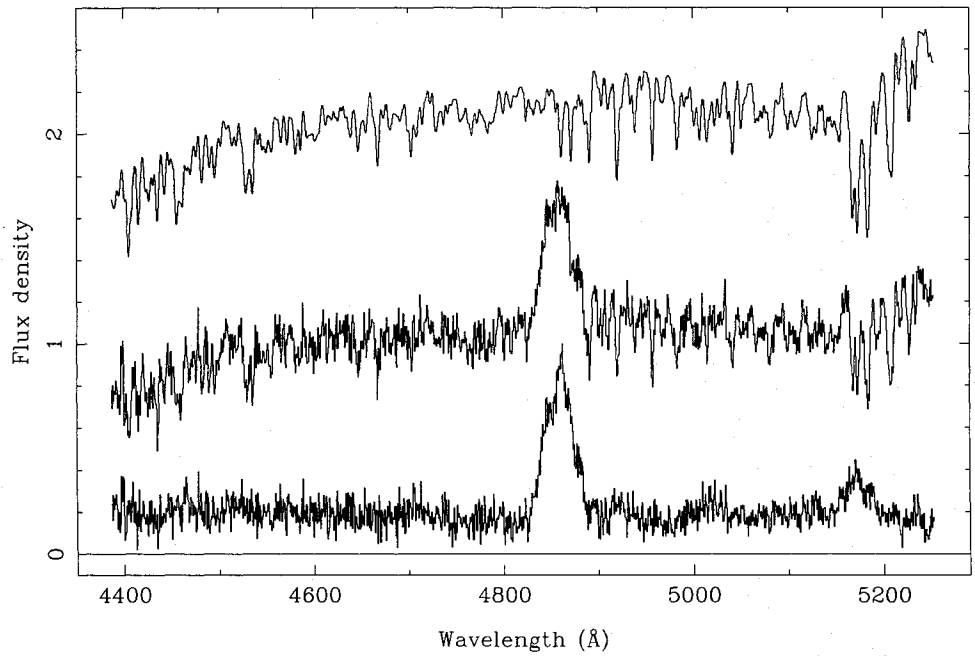

Figure 3. As Fig. 2, but now for the blue-side data.

The equivalent width of the line in our spectra is 160 ± 30 mÅ (corrected for the disc's contribution), with the uncertainty dominated by the uncertainty in placing the continuum. For comparison, Martin et al. (1992) found 290 ± 50 mÅ in V404 Cyg.

The blue spectrum reveals lines redward of Hβ which, judging by the weakness of He I 4471 and the presence of the line at ≈ 5170 Å, are not He I emission lines but multiplet 42 of Fe II at 4924, 5018 and 5169 Å (Moore 1972). There is no He II 4686 emission and, given the weakness of the He I lines, the overall impression is of a spectrum very similar to those of dwarf novae in quiescence, but of lower excitation.

In Figs 4 and 5 we show the spectrum of A0620−00 in the heliocentric rest frame, which is almost that of the compact object as well. The template was subtracted from the individual spectra with the correct radial velocity, and normalized according to a fit to ellipsoidal variations (see next section). The strong, double-peaked Balmer lines are one of the characteristic signatures of accretion discs in dwarf novae, and presumably in A0620−00 as well. Measurements on some lines are listed in Table 3. The equivalent width of Hα emission from the disc is remarkable, although there is considerable uncertainty in the precise value because of the large fractional uncertainty in the disc's contribution.

3.4 Ellipsoidal variations in the equivalent width of Hα

Fig. 6 shows the equivalent width of Hα for the 51 spectra versus orbital phase (without subtraction of the secondary star spectrum). The equivalent width is maximum at the conjunction phases and minimum at quadrature. Since the K star dominates the continuum, the obvious interpretation is that the Hα flux from the disc is roughly constant but the K star suffers ellipsoidal variations, producing least light when its projected area is minimum at conjunction, and most when seen at quadrature. The variations in the continuum will be seen in reverse in the equivalent width of Hα. We have no independent proof that the Hα flux from the disc is constant, since our data are not photometric, but the agreement between the variations of Fig. 6 and those expected from ellipsoidal variations must otherwise be dismissed as coincidental.

Ellipsoidal variations, which have been seen before in A0620−00 (MR; Haswell et al. 1993), vary with mass ratio and orbital inclination of the binary. We measured the amplitude of the variations by fitting a sinusoid with a frequency twice that of the binary, and phased to peak at conjunction. We found that the equivalent widths could be fitted with

$$\mathrm{EW(\AA)} = (61.4 \pm 0.6) + (7.8 \pm 0.8) \cos 4\pi\phi,$$

which is plotted in Fig. 6.

Correcting for the contribution from the disc, which we assume to be constant, we obtain a semi-amplitude of the ellipsoidal variations of 0.13 ± 0.02 mag. We will discuss the constraint on the inclination in a later section. We used our fit to normalize the A0620−00 spectra and to compute the correct factor when removing the template star spectrum (Figs 4 and 5).

If our interpretation of the variations in Hα flux is correct, then the grazing eclipse of the K star by the disc, seen by Haswell et al. (1993), which would be evident as an increase in the equivalent width at phase 0.5, is no longer present.

3.5 Doppler images of Hα and Hβ

The emission lines from cataclysmic variables are broadened by Doppler shifting from the accretion disc, component stars and mass transfer stream. Marsh & Horne (1988) have shown how it is then possible to derive the distribution of emission from observations of the profile covering the binary orbit. Doppler images for the dwarf novae IP Peg and U Gem

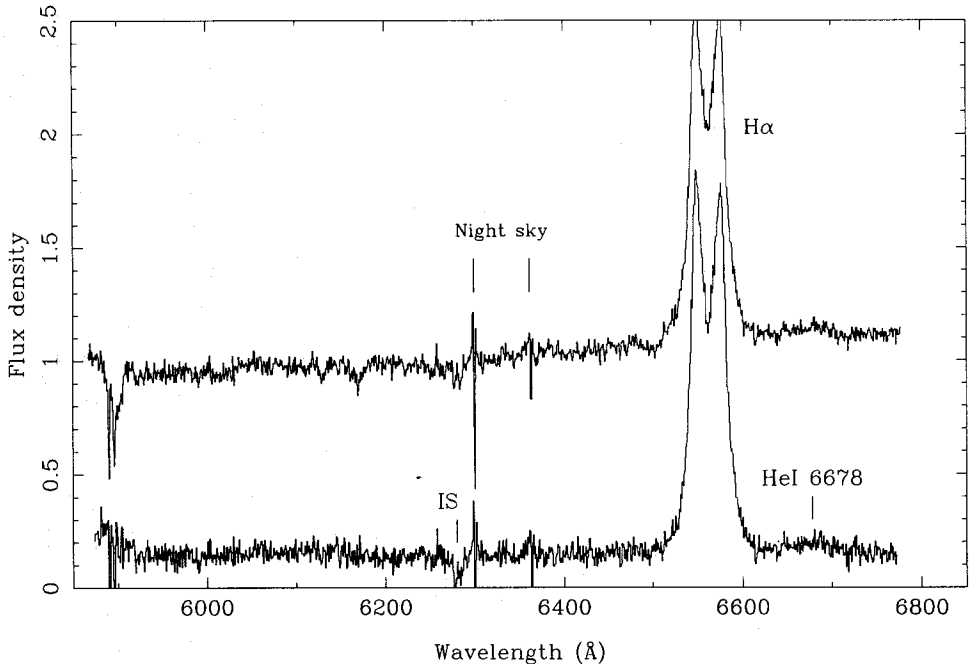

Figure 4. The average spectrum of A0620−00 in our rest frame is plotted along with the same spectrum after subtraction of the K star from each spectrum before averaging. The result is the spectrum of the disc and bright-spot. Apart from the strong Hα line, weak He I 6678 and possibly He I 5876 emission is visible. For reference, before sky subtraction, the brightest night-sky line at 6300 Å was 100 times brighter than A0620−00 over the spatial extent of the stellar image.

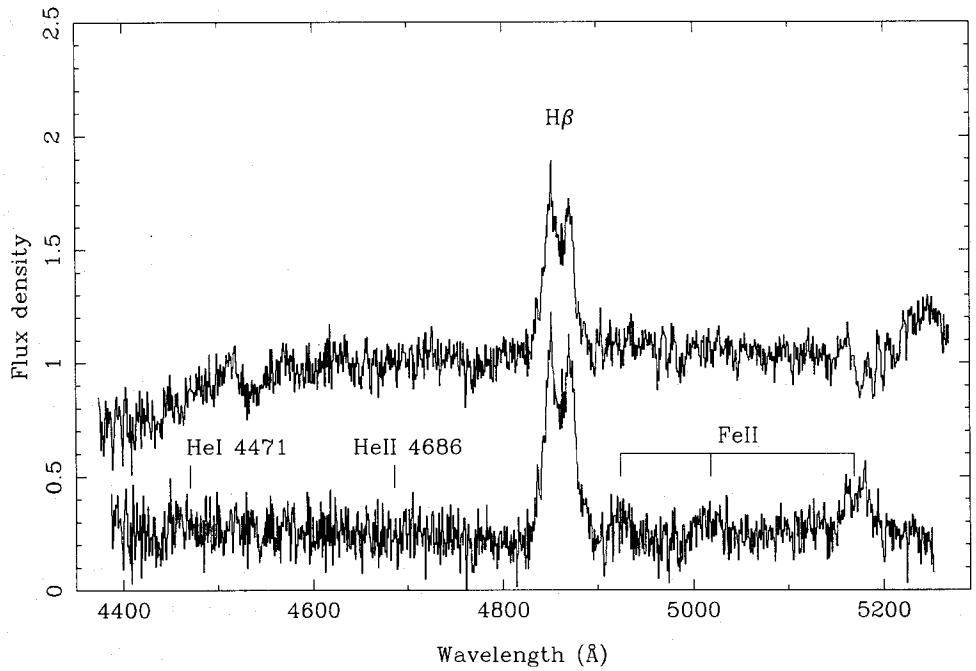

Figure 5. As Fig. 4, but now for the blue-side data. The lines redward of Hβ are from the Fe II multiplet 42 and not He I, since He I 4471 is very weak.

have been presented by Marsh & Horne (1990) and Marsh et al. (1990), and we now apply the same method to A0620−00.

After the K-star spectrum had been removed, we fitted and subtracted straight lines from the continuum near Hα and Hβ. We then computed Doppler images of the lines, which are displayed in Figs 7, 8 and 9. The left-hand panels of Fig. 7 show the result for Hα, with the raw data at the top, the image in the middle and the fitted data in the lower panel. In the right-hand panels, the same data are displayed after subtraction of the azimuthally symmetric part of the image centred upon the centre of mass of the compact object at $(0, -K_1)$, where $K_1 = qK_2 = 29$ km s^{-1} (we attempt to measure this directly in the following section).

Table 3. Emission-line parameters.

	Hα	Hβ	HeI 6678	HeI 4471	HeII 4686
EW (Å) (K star present)	58 ± 1	22 ± 2	2.4 ± 0.3	0.5 ± 0.3	1 ± 0.5
EW (Å) (disc only)	970^{+1000}_{-300}	130 ± 20	40^{+40}_{-12}	3 ± 2	5 ± 3
FWZI ($\mathrm{km\,s^{-1}}$)	5000 ± 150	4600 ± 200	—	—	—
FWHM ($\mathrm{km\,s^{-1}}$)	1900 ± 50	2260 ± 150	—	—	—
Peak separation ($\mathrm{km\,s^{-1}}$)	1270 ± 60	1200 ± 150	—	—	—

Note: the uncertainty in the disc's continuum is included in the equivalent widths of Hα, Hβ and He I 6678, but not in the non-detections for He I 4471 and He II 4686.

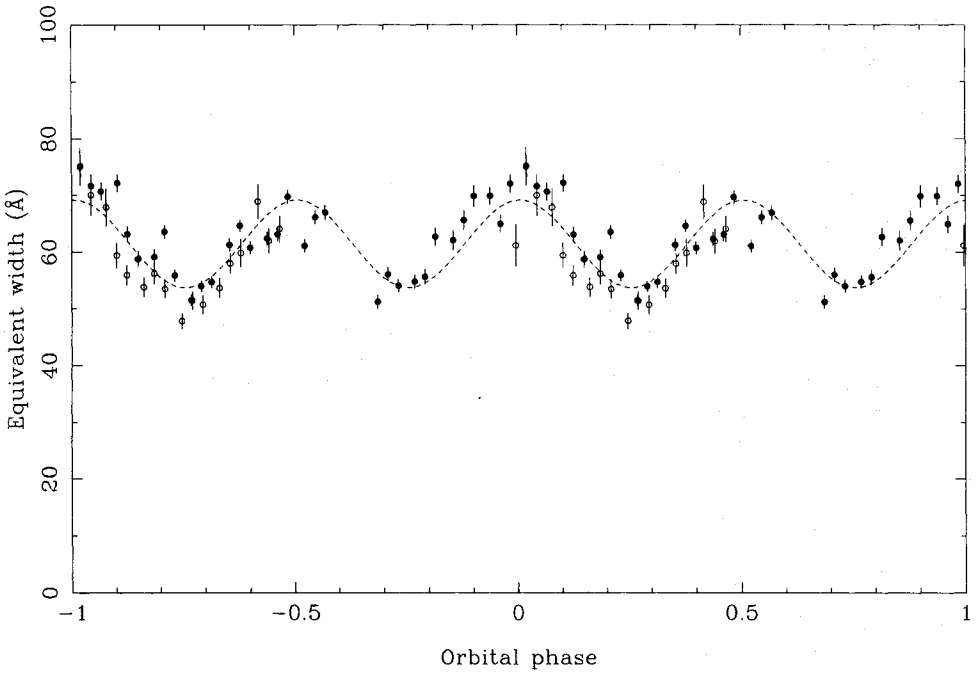

Figure 6. The equivalent widths of Hα are plotted as open circles for the first night, and filled circles for the second. The dashed line is a fit of a sinusoid plus a constant, assuming that the variations are caused by 'ellipsoidal' variations of the secondary star. The period and phasing of the sinusoid were held fixed during the fit.

The images are presented in velocity rather than position coordinates, since there is no unique transform between velocity and position in accreting binaries (in contrast to rapidly rotating, single stars, for example). The result is a little peculiar, with the region closest to the compact object transformed to the outermost parts of the image as they move at high velocity. Equally, the centre of the image, which is at zero velocity, represents a forbidden zone where no emission should be seen, unless there are non-Doppler broadening mechanisms present. It is straightforward to predict the positions of the various components in velocity coordinates. In Figs 7, 8 and 9, paths for the gas stream and the velocity of the disc along the gas stream have been drawn for $K_2 = 433$, $q = 0.067$. The broad, ring-shaped background is the emission from the accretion disc which extends to high velocities. Emission is seen on and near the secondary star, and it extends along the path of the stream to reach maximum intensity where it hits the disc.

The bright-spot is not placed on either predicted path for the gas stream, but occurs roughly half-way between them, as was found for U Gem (Marsh et al. 1990). Smaller mass ratios bring the predicted paths closer to the spot, but the available range of q is not sufficient to obtain agreement. As for U Gem, this suggests that we are seeing emission from material after it has passed through the shock at the edge of the disc. Prior to the shock, the emission has the velocity of the gas stream alone, as is to be expected. If we assume that the velocity after the shock is a linear combination of the disc and gas stream velocities at every point, then we can deduce a radius for the post-shock emission. We find that it is concentrated at a radius of $0.5 \pm 0.05\, R_{\mathrm{L1}}$; the spread may be an effect of finite spectral resolution and signal-to-noise ratio rather than a true variation. Emission extends to high velocities from the bright-spot region, corresponding to emission seen at high velocities in the blue wind of the data. We do not know what causes this emission, but note that it can be expected to distort measurements of the compact object's radial velocity (Section 3.6).

Some of the emission on the K star seen in Fig. 7 is a result of subtraction of the absorption line of Hα in the template. How much cannot be estimated directly from the image, as the maximum-entropy method used in generating it tends to

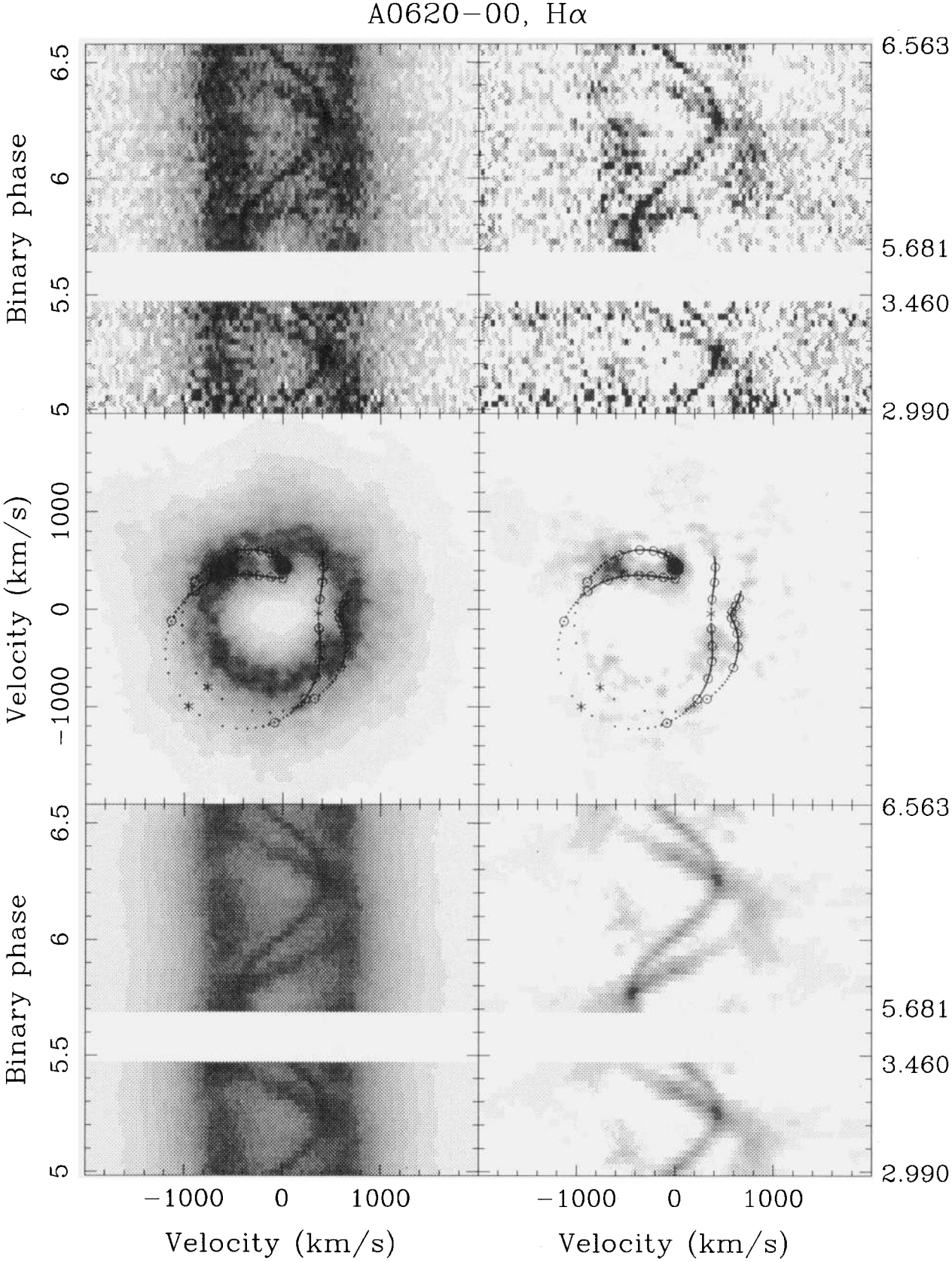

Figure 7. The Doppler images of Hα after subtraction of the K-star spectrum. The left-hand panels show, from the top, the data, the image and the fitted data. A gap has been inserted between the first night's data in the lower half of the data panels and the second night's data in order to maintain the correct phases. However, two cycles have been removed from the gap to avoid compression of the trailed spectra. The right-hand panels show the result after subtraction of the axisymmetric part of the image. The predicted velocities of the gas stream (which starts from the inner Lagrangian point) and of the disc along the gas stream are plotted for $K_2 = 433$ km s^{-1} and $q = K_1/K_2 = 0.067$. Asterisks mark turning points in distance from the compact object. Circles have been plotted every 0.1 R_{L1}, and dots every 0.01 R_{L1} along the streams.

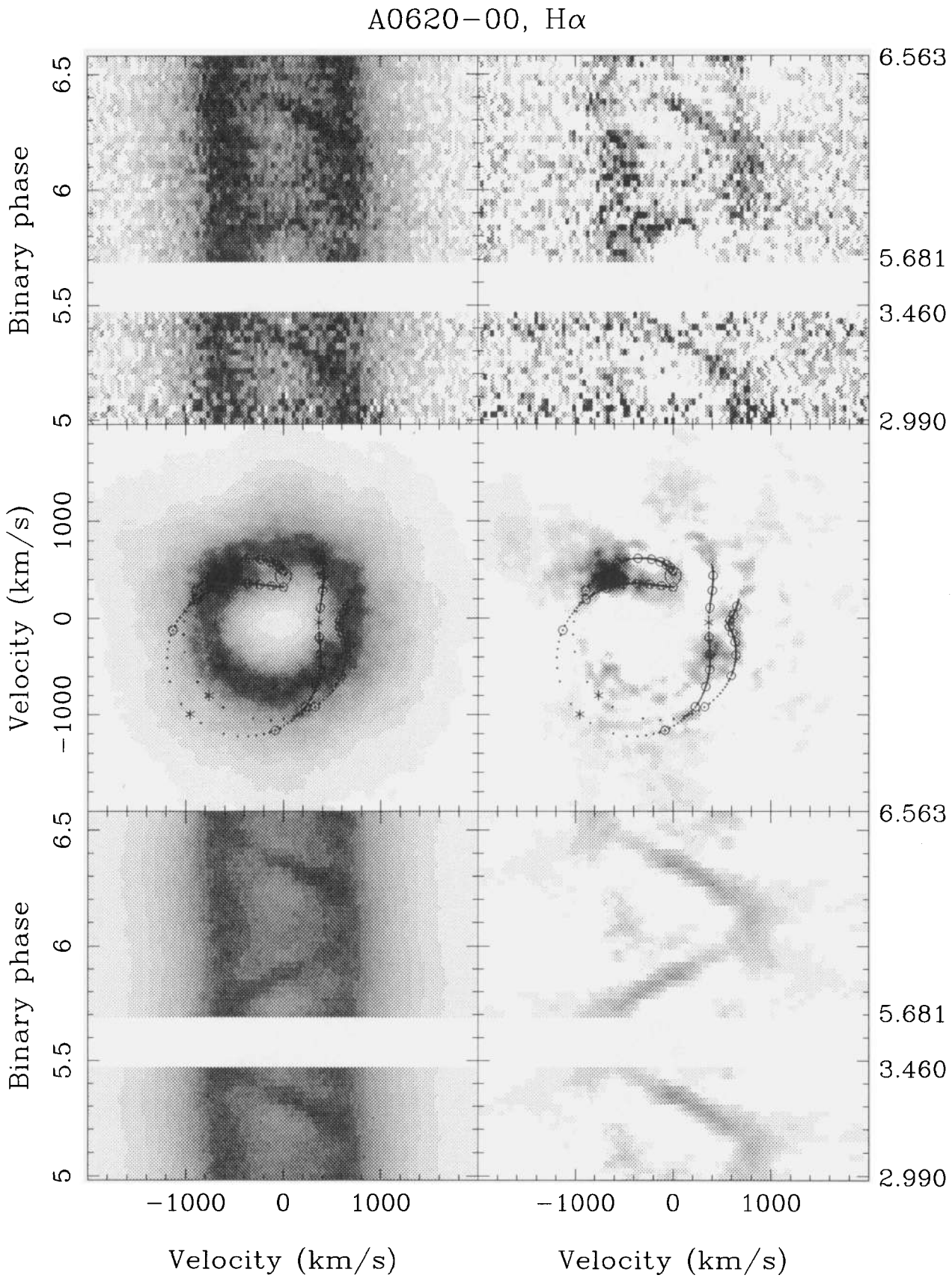

Figure 8. As Fig. 7 but, before subtracting the K star, its Hα absorption line was removed by interpolation, in order to assess the true strength of emission from the secondary.

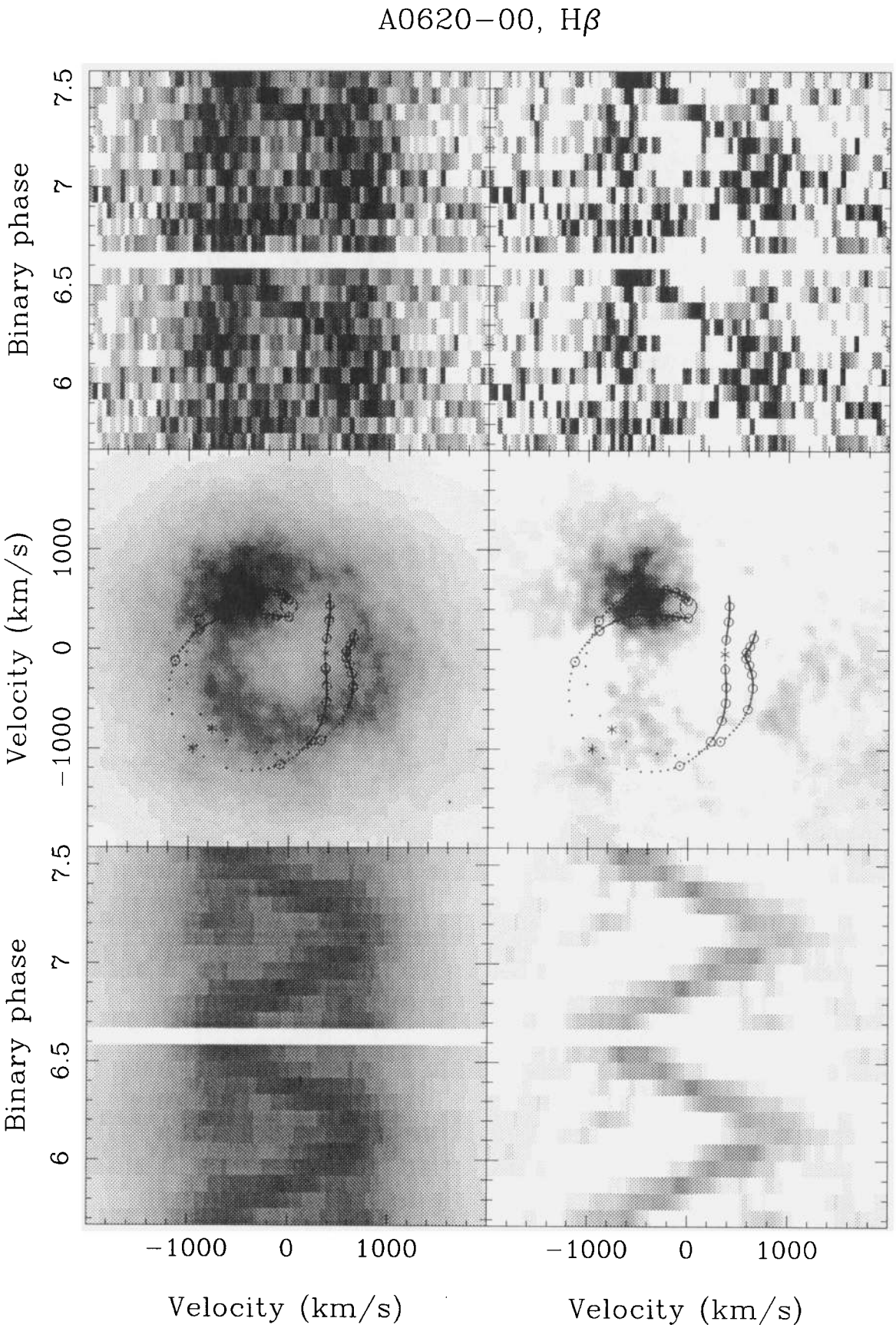

Figure 9. This figure shows the equivalent of Fig. 8 for Hβ. In other words, the Hβ line was removed from the template before subtraction. In this case, the 11 blue spectra have been plotted twice with a gap, since the blue spectra are from one night only and do not cover a full orbit.

suppress sharp peaks. Instead, we removed Hα from the template by interpolating across it prior to subtraction, and recomputed the image. The result is shown in Fig. 8. While weak emission remains on the red star, a comparison of Figs 7 and 8 shows that essentially all the emission on the K star in Fig. 7 is caused by subtraction of the template's absorption line. If a spectrum of the K star could be taken with no contamination from the disc, Hα would be seen to be filled in, perhaps as a result of its rapid rotation. It is not clear whether this can be described in terms of an emission-line layer separate from an underlying photosphere, and thus we cannot pick one of Figs 7 and 8 as the 'correct' image of the K star. We can say that in no way does the emission in Fig. 7 provide us with any new information as to the rotational broadening of the K star, since it depends entirely upon the broadening applied to the template, and therefore we marginally prefer Fig. 8 as a less misleading representation of the spectra.

Fig. 9 is the equivalent for Hβ of Fig. 8, with the Hβ in the template removed before subtraction. We do not show the case with strong emission from the red star since, at the poor signal-to-noise ratio of the blue data, the emission from the K star merges with the emission from the bright-spot, and it is the latter that is of more interest here. The maximum intensity in Hβ appears to be a bit further out, at $\approx 0.6\,R_{L1}$. Data of higher signal-to-noise ratio are needed to be sure of this, however. The bright-spot's emission in Hβ relative to that from the disc is stronger in comparison to Hα by a factor of ≈ 2.5, which suggests that it is coming from more optically thick material than the disc. Otherwise, the Hβ image is similar to the Hα image.

If we assume that the velocity field of the disc is Keplerian, we can transform our images from velocity to spatial coordinates. The results, taking $K_2 = 433$ km s^{-1}, $q = 0.067$, $i = 70°$, and a distance of 485 pc (see below), are plotted in Fig. 10. An absolute scaling was not possible because of the non-photometric conditions; the vertical scale of Fig. 10 is based on our normalization of the spectra to have a continuum of 1 mJy. Since the contribution of an annulus in the disc to the total flux in the line is proportional to $2\pi RI\,\mathrm{d}R = 2\pi R^2 I\,\mathrm{d}\ln R$, where I is the surface brightness and R the radius, we have plotted $\log(R^2 I)$, rather than $\log I$, versus $\log R$. Beyond the edge of the disc, the results are sensitive to optical-depth effects which we have not accounted for, and thus the apparent emission from radii larger than the binary separation is not significant. At very small radii, noise corrupts the results, leaving the zone from 6×10^9 to 10^{11} cm as reliable. In this region $R^2 I$ is approximately proportional to R, and so $I \propto 1/R$. This is comparable to, although less steep than, the behaviour seen in dwarf novae for which typically $I \propto 1/R^{1.5}$ (Horne & Saar 1991). Fig. 10 shows that Hα strengthens relative to Hβ in the outer parts of the disc, and this has also been seen in dwarf novae (Marsh et al. 1990).

3.6 Measurement of the emission-line radial velocities

In studies of cataclysmic variables, it is common to assume that radial velocities of the emission lines reflect the radial velocity of the accreting object K_1. In the case of A0620−00, we believe that the mass ratio derived in Section 3.2 provides a more reliable estimate of $K_1 = qK_2 = 29$ km s^{-1}, but it is still worthwhile to attempt the direct measurement.

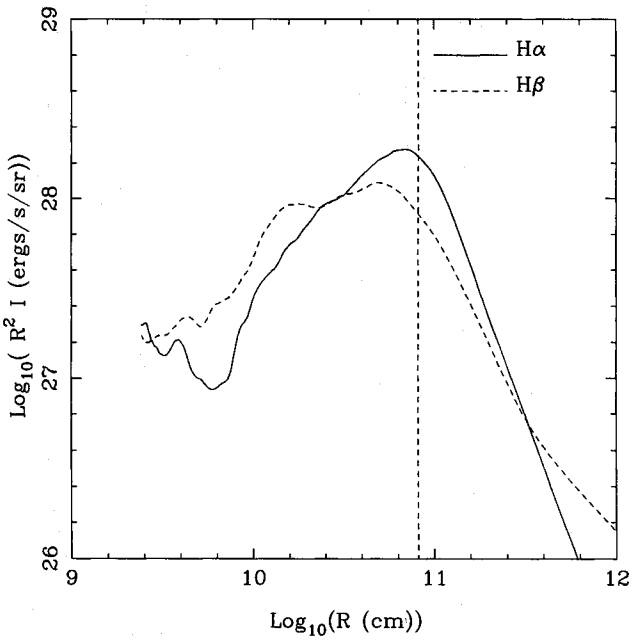

Figure 10. The log of the surface brightness of the disc, I, times the square of the radius, R, is plotted for Hα and Hβ against log radius. We plot $R^2 I$, since it represents the contributions of different radii to the total line flux correctly. The vertical dashed line marks a radius of $0.5\,R_{L1}$.

We apply the usual double-Gaussian method of Schneider & Young (1980) and Shafter (1983), but with one modification. Normally, the velocities are measured for each spectrum and then fitted with a circular orbit to obtain the amplitude, phase and systemic velocity for a series of different separations of the two Gaussians. This method is noise-sensitive in that, while only three parameters are required in the end, the intermediate stage may involve 20 or 30 parameters (i.e., a velocity for each spectrum). Often it becomes impossible to measure the velocities of some of the spectra, and these spectra have to be eliminated from the fit, possibly biasing the results. In order to avoid this problem, we fitted circular orbits directly to the data by minimization of χ^2, defined by

$$\chi^2 = \sum_i \frac{\left[\sum_j g_{ij} D_{ij}\right]^2}{\sum_j g_{ij}^2 \sigma_{ij}^2},$$

where D_{ij} and σ_{ij}^2 are the datum and variance for the jth point of the ith spectrum, and g_{ij} is the value of the double-Gaussian function for the same point. For a Gaussian separation of a and standard deviation σ, g is given by

$$g_{ij} = \exp\left[-\frac{(V_j - U_i - a/2)^2}{2\sigma^2}\right] - \exp\left[-\frac{(V_j - U_i + a/2)^2}{2\sigma^2}\right],$$

where V_j is the velocity of the jth pixel relative to the rest wavelength of the line in question, and U_i is the predicted velocity of the ith spectrum according to

$$U = \gamma - K_X \sin 2\pi\phi + K_Y \cos 2\pi\phi.$$

The parameters γ, K_X and K_Y are the fitting parameters, and we determine them, and their errors, using standard techniques (Press et al. 1986). As we have defined χ^2, the numerator of the fraction inside the first summation is the square of the function that is usually set equal to zero during iteration to find a specific spectrum's velocity, and the denominator is its variance.

The results of this measurement are the same as those of the usual method in cases when the latter works, but the modified method is not upset by a particularly poor spectrum or two. We list the results for $\sigma = 100$ km s^{-1} and separations ranging from 1400 to 2900 km s^{-1} in steps of 100 km s^{-1} in Table 4. The results are plotted in Fig. 11, in two panels, with the right-hand panel an expanded version of the left-hand panel. As discussed in Marsh (1988), the points represent the mean of flux at $\approx \pm a/2$ from the centre of the line. For the separations plotted in Fig. 10, such emission is outside the plot area of even the left-hand panel, and therefore it is not very surprising that the results are strongly distorted.

The predicted value of $K_1 = 29 \pm 4$ km s^{-1} is plotted in Fig. 11. The points progress towards this value, but are corrupted by noise some way before the V_Y axis is reached. The points are offset towards the bright-spot emission seen in Figs 7, 8 and 9, and they do not give a reliable value of K_1. Marsh (1988) tried to correct similar data on IP Peg by extrapolation towards the vertical axis. Taking the points before noise begins to dominate, this method gives $K_1 \approx 35$ km s^{-1} for A0620−00, but it is less reliable in this case, as the distortion is still large when statistical noise starts to dominate. Haswell & Shafter (1990) have also measured the radial velocity variations of the compact object, and their radial velocities are distorted in the same manner as ours. Haswell & Shafter's measurement (43 ± 8 km s^{-1}) and our measurement (35 km s^{-1}) of K_1 from the emission lines, compared to our estimate of 29 km s^{-1} based upon $v \sin i$, indicate that Haswell & Shafter's suggestion that the bright-spot distortion will lead to an underestimate of K_1 is not always correct.

We conclude that distortion by emission from the bright-spot and other asymmetries renders the emission-line radial velocities unreliable for estimating K_1, and instead we use the value deduced from the rotational broadening of the secondary star.

Table 4. Hα radial velocity fits.

Separation km s^{-1}	χ^2	γ km s^{-1}	K_X km s^{-1}	K_Y km s^{-1}	R_{XY}
1400	92	−3.5±6	−29.9±7	4.3±9	0.265
1500	82	1.4±4	−33.0±5	−7.4±6	0.209
1600	70	2.4±3	−34.5±4	−11.6±5	0.161
1700	60	2.0±3	−35.2±3	−14.0±4	0.104
1800	54	0.8±3	−34.2±3	−16.4±4	0.047
1900	49	−0.6±3	−31.0±3	−19.7±4	0.009
2000	42	−1.5±3	−26.2±4	−23.9±4	0.002
2100	37	−1.4±3	−21.2±4	−27.6±4	0.033
2200	36	−0.2±4	−17.7±5	−29.1±5	0.082
2300	39	1.9±4	−16.6±6	−28.1±6	0.088
2400	43	4.7±5	−17.9±8	−26.5±7	0.036
2500	48	7.2±6	−19.4±9	−25.4±8	0.011
2600	51	7.8±7	−17.6±10	−24.8±9	0.045
2700	51	7.9±7	−12.8±11	−26.4±10	0.077
2800	50	11.2±8	−12.3±14	−31.6±10	0.151
2900	51	18.1±10	−19.7±26	−40.5±11	0.365

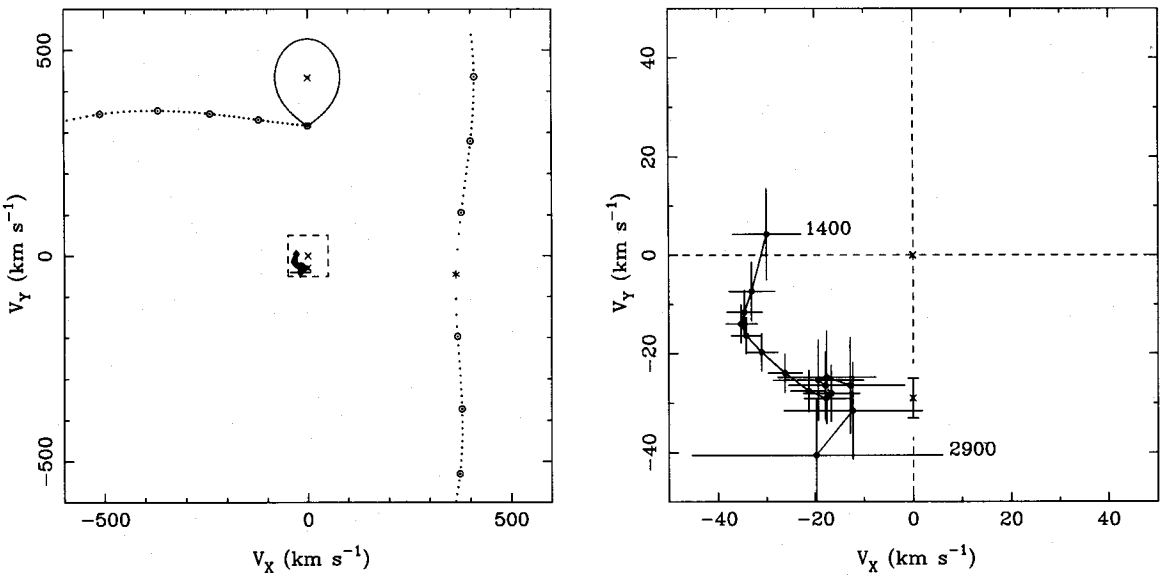

Figure 11. The light centres obtained from double-Gaussian fits to Hα, with the separation varying from 1400 to 2900 km s^{-1} in steps of 100 km s^{-1}, are plotted in velocity coordinates. The left-hand panel plots them in the context of other components of the binary, with $K_2 = 433$ km s^{-1} and $q = 0.067$, and the right-hand panel shows an expanded view of the region of the left-hand panel enclosed by the dashed square. Crosses mark the centre of mass of the K star at (0,433), the centre of mass of the system at (0,0) and the best estimate for the centre of mass of the compact object at $(0, -29 \pm 4)$.

4 DISCUSSION

4.1 Parameter estimates

Our values of $K_2 = 433 \pm 3$ km s^{-1} and $q = 0.067 \pm 0.01$, combined with the orbital period and the binary inclination i, give the masses of the compact object and its companion, M_1 and M_2:

$$M_1 = \frac{3.09 \pm 0.09}{\sin^3 i}\,\mathrm{M}_\odot, \qquad M_2 = \frac{0.21 \pm 0.04}{\sin^3 i}\,\mathrm{M}_\odot.$$

The best constraint upon the inclination comes from the observation of Haswell et al. (1993) of a grazing eclipse of the K star by the disc. Before applying this, we consider the independent constraints from our own data.

A firm upper limit upon i can be deduced from the absence of any rotational disturbance in Hα, as first the blueshifted and then the redshifted peak would be eclipsed if the outer disc were obscured by the secondary star (Greenstein & Kraft 1959; Young & Schneider 1980). The Hα emission is likely to be more sensitive to eclipses than the continuum, since the latter is dominated by the K star. Using the disc radius of $0.5\,R_{\mathrm{L1}}$ from the Doppler images, we deduce that the inclination must be $\lesssim 76°$.

If we take the ellipsoidal variations of Section 3.4 at face value, another constraint can be deduced. McClintock et al. (1983) and others have used the following formula, due to Russell (1945), which gives the semi-amplitude of the ellipsoidal variations for a tidally distorted star as

$$\Delta m \approx \frac{3}{4q}\left(\frac{R_2}{a}\right)^3 \sin^2 i (1+\tau)\,\frac{15+u}{15-5u}\,\mathrm{mag},$$

where R_2 is the radius of the companion star and a the separation, τ is the gravity-darkening coefficient, and u is the linear limb-darkening coefficient (our definition of $q = M_2/M_1$ is inverted with respect to Russell's). The gravity-darkening coefficient τ is 4 times the coefficient β used earlier, and therefore we take $\tau = 0.32$; however, as we remarked earlier, it could be as small as 0 (Anderson & Shu 1977). Using Paczyński's (1971) formula for R_2/a of stars filling their Roche lobes, and $u = 0.65$, we obtain $\Delta m = 0.13 \sin^2 i$. This matches our measurement of 0.13 ± 0.02 mag; however, Russell's formula underestimates the amplitude of the ellipsoidal variations, since the approximations he used become inaccurate for a star filling its Roche lobe (Bochkarev, Karitskaya & Shakura 1979). We corrected for this by carrying out simulations with the program already used in Section 3.2, which also allowed us to include quadratic limb darkening as before. Results for the linear and quadratic limb-darkening coefficients of $a = 0.6$ and $b = 0.2$ are listed in Table 5 for two models: (i) with $\tau = 4\beta = 0.32$, and (ii) with $\tau = 4\beta = 0$. For comparison with Russell's formula we also list $\Delta m/\sin^2 i$, which can be seen to be larger than his analytic formula (as well as variable).

Table 5. Models of ellipsoidal variations.

i	Δm	$\Delta m/\sin^2 i$	Δm	$\Delta m/\sin^2 i$
	mags, $\tau = 0.32$		mags, $\tau = 0.00$	
90°	0.213	0.213	0.154	0.154
80°	0.205	0.212	0.149	0.154
70°	0.183	0.207	0.135	0.153
60°	0.151	0.201	0.113	0.151
50°	0.114	0.194	0.088	0.150
40°	0.077	0.186	0.061	0.148
30°	0.045	0.179	0.036	0.145

Combining the eclipse and ellipsoidal constraints, for $\tau = 0.32$, we find a best-fitting value of 54°, with ranges of $48° < i < 60°$ (1σ) and $43° < i < 66°$ (2σ) while, for $\tau = 0$, the best fit is 67° with ranges $58° < i < 76°$ (1σ) and $51° < i < 76°$ (2σ). Given the uncertainty on τ, these results are consistent with the fits of Haswell et al. (1993), who found $66.^\circ5 < i < 73.^\circ5$ for $q = 0.067$. Their constraint upon i, based as it is upon the observation of an eclipse, should be relatively insensitive to τ. Given the agreement, we take Haswell et al.'s constraint as the more accurate and precise. Taking the extreme limits of the range for i given by Haswell et al., we obtain ranges for the masses of

$$3.89 < M_1 < 4.12\,\mathrm{M}_\odot, \qquad 0.19 < M_2 < 0.32\,\mathrm{M}_\odot,$$

for 1σ deviation from the masses quoted at the start of this section, and

$$3.30 < M_1 < 4.24\,\mathrm{M}_\odot, \qquad 0.15 < M_2 < 0.38\,\mathrm{M}_\odot,$$

for a 2σ deviation. The uncertainty in the mass of the K star, M_2, is dominated by the uncertainty in the mass ratio q, whereas the uncertainty in the mass of the compact object is dominated by the inclination, which itself hinges upon the identification of the eclipse by Haswell et al. (1993).

The 2σ lower limit of $3.30\,\mathrm{M}_\odot$ is higher than the maximum mass of a rotating neutron star of $3.2\,\mathrm{M}_\odot$ found by Friedman, Ipser & Parker (1986) for their stiffest equation of state (rotation and stiff equations of state both increase the maximum mass). However, the equation of state of neutron stars is not well understood and, if only a causality limit is applied, the maximum possible mass might be larger than our mass (Friedman & Ipser 1987).

The companion star has a spectral type in the range K3 to K4 (Haswell et al. 1993), and main-sequence stars of this spectral type have masses of about $0.7\,\mathrm{M}_\odot$. Such a mass is possible only if the orbital inclination is $\approx 45°$, contrary to Haswell et al.'s observation of an eclipse. This may not present any problem if the secondary star is somewhat evolved (cf. King 1993). If, as our mass estimate suggests, the K star is not on the main sequence, Oke's (1977) estimate of a distance of 870 pc to A0620 − 00, which was based upon the assumption of an absolute magnitude appropriate for a K dwarf, must be revised. We now derive a more general estimate using the Barnes–Evans relation (Barnes & Evans 1976).

Adapting the revised fits of Eaton & Poe (1984) for stars with dereddened $V-R$ colours in the range $0.67 < (V-R)_0 < 1.65$, we find the following expression for the angular diameter of the K star in milliarcsec, θ:

$$5 \log \theta = 3.19 + 3.55(V-R)_0 - V_0,$$

where V_0 is the dereddened apparent visual magnitude. Using a ratio of total-to-selective extinction of $A_V/E(B-V) = 3.1$ (Rieke & Lebofsky 1985) and a colour $(V-R)_0 = 0.9$, appropriate for a K3 dwarf, and setting $E(B-V) = 0.4$, we find

$$\log \theta = 1.525 - V/5.$$

Haswell et al. (1993) find $V \approx 18.2$, but only half of this light is from the K star; so we use instead $V \approx 18.9$. The radius of the red star is a function of the separation of the binary components and the mass ratio, and therefore we can deduce the distance d, which is

$$d = \frac{0.46 q^{1/3}(1+q)^{2/3} K_R P}{2\pi\theta \sin i}.$$

Putting $q = 0.067$, $K_R = 433$ km s^{-1}, $P = 0.323\,014$ d and $V = 18.9$ in the expression for θ, we find $d = 456/\sin i$ pc. As expected, this is close to Oke's (1977) estimate for low inclinations which also bring the mass of the K star closer to the main-sequence value. Haswell et al.'s (1993) inclination of $i \approx 70°$ gives $d \approx 485$ pc.

4.2 Comparison with previous observations

Comparable studies of the Hα emission have been made by Johnston et al. (1989) and by Haswell & Shafter (1990). Johnston et al. (1989) found an asymmetry in the disc's emission, which they modelled with a variation in intensity as a function of azimuth ψ in the disc (measured in a prograde direction from the red star) of the form $1 + \beta\cos(\psi - \psi_{hs})$. They found that the bright-spot led the red star by only $\psi_{hs} = 7°$, and also that a delta function for the bright-spot was too sharp to fit the data well. They used a fit to the line profile, from which they obtained a value of 540 km s^{-1} for the outer disc velocity, to constrain q to be < 0.01, and deduced an unusual picture of the system in which the disc almost fills its Roche lobe so that the bright-spot would be placed close to the K star, in agreement with the small value of ψ_{hs}.

There are several problems with Johnston et al.'s analysis. First, a fit in which the disc is brighter at a particular azimuth over all radii is not a good approximation to the asymmetries seen in Figs 7 and 8. The selection of a cosine behaviour limits the fit to large-scale asymmetries only, whereas the bright-spot is confined to a small range in azimuth. It is not clear what azimuth would be obtained from such a fit, but it may bear little relation to the position of the bright-spot. Johnston et al. constrained the mass ratio q from the ratio of the outer disc velocity to the semi-amplitude of the K star, V_{disc}/K_2, which they found to be 1.17, and found that $\mu = q/(1+q) < 0.048$ for the disc to have a radius, R_{disc}, less than the distance to the inner Lagrangian point, R_{L1}. For Keplerian velocities, it can be shown that

$$\frac{V_{disc}}{K_2} = \sqrt{\frac{a}{R_{disc}(1+q)}},$$

where a is the binary separation. Setting $R_{disc} = R_{L1}$, we find that $V_{L1}/K_2 < 1.13$ for all q, and therefore there appears to be no problem in matching the observed value of 1.17.

As Johnston et al. point out, tidal forces from the secondary star will prevent the disc from approaching the inner Lagrangian point. As a better approximation, Johnston et al. took the largest non-intersecting orbit as the largest possible radius for the disc, following Paczyński (1977). They then found that $\mu < 0.01$, a very extreme mass ratio which is inconsistent with our rotational broadening. However, Johnston et al.'s predicted value of V_{disc}/K_2 is never low enough to match their measured value, so it is not clear that their result is justified. In fact, the low outer-disc velocity in Johnston et al.'s data is probably an artefact of low resolution, as Fig. 12 demonstrates. Here we compare our Hα profile with that of Johnston et al., in the top panel directly, and in the lower panel after blurring and binning to match Johnston et al.'s resolution. In the top panel, it appears that the peaks have a significantly higher velocity in our data, indicating a contraction of the disc in the six-year interval between the two data sets. However, our blurred profile in the lower panel has almost exactly the same peak separation as Johnston et al.'s data, and so there is no evidence for a change in disc size between the two data sets. The dashed lines which represent a disc radius of $0.5\,R_{L1}$, derived from our Doppler images, run close to the peaks, although there might still be some bias caused by finite resolution. In summary, the emission-line peak separation in both data sets is consistent with our mass ratio, and suggests a disc radius in the range 0.5 to $0.6\,R_{L1}$.

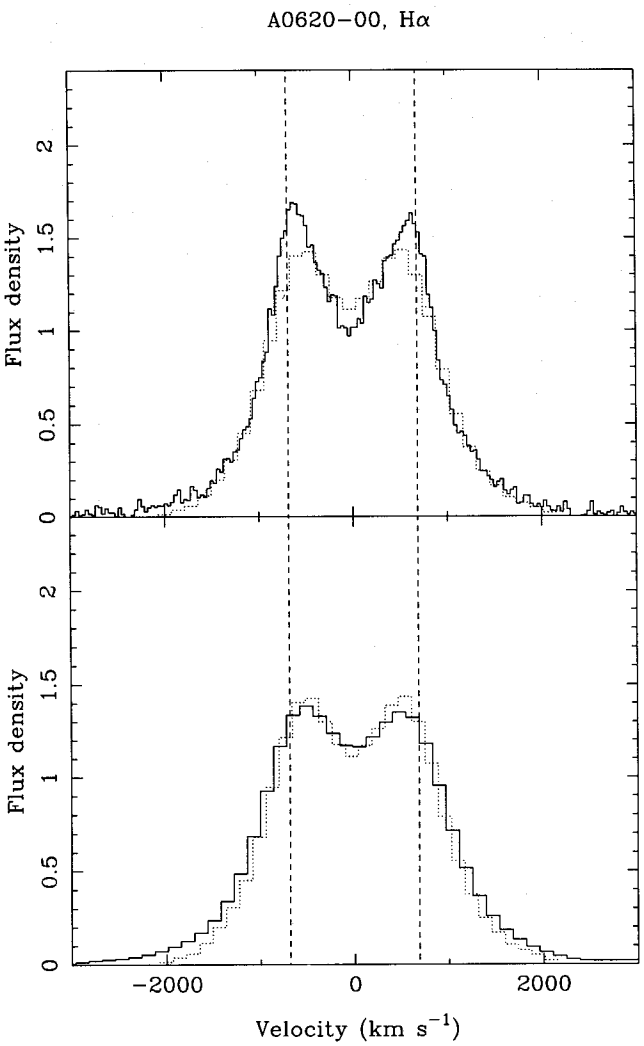

Figure 12. The upper panel shows the profile of Hα we observed (solid line), together with the profile of Johnston et al. (1989). The same data are plotted in the lower panel, but now the solid line represents our data after it has been blurred and binned to match Johnston et al.'s data. The dashed lines show the outer edge velocity for $R_{disc} = 0.5\,R_{L1}$, as suggested by our Doppler images.

Haswell et al. (1993) discuss data taken eight months after Johnston et al. (1989) and, in order to fit an eclipse of the K star, they require disc radii ranging from 0.7 to $0.85\,R_{L1}$. This might imply that the disc radius is variable, or it might be a consequence of differing methods for measuring the disc radius, since Haswell et al.'s data measure the radius of optically thick material in the outer disc, rather than the radius of the Hα region.

4.3 Accretion rate in the inner disc

In dwarf novae He II 4686 flux is thought to be produced by photoionization by radiation from the boundary layer (at normal accretion rates the inner disc is too cool to have much effect) (Patterson & Raymond 1985; Marsh & Horne 1990). We could not detect any He II 4686 flux in the spectrum of A0620−00, which indicates that there is little ionizing flux in the system. As black holes do not have boundary layers, this might not seem to tell us much, but, because the black hole in A0620−00 is so much smaller than a white dwarf, temperatures in the inner disc can become high enough to produce photoionizing radiation at relatively low accretion rates. Therefore the absence of He II 4686 constrains the accretion rate in the inner disc, rather than the presence of a boundary layer. We now carry out a rough estimate to see whether or not this constraint is significant.

We assume that every photon incident upon the accretion disc with energy in the range $55 < h\nu < 280$ eV defined by the ionization energy of He I and the carbon K-edge causes one photoionization of He I. A fraction ε of subsequent recombinations produce a He II 4686 photon, and we take $\varepsilon = 0.2$, appropriate for Case B recombination (Hummer & Storey 1987). The fraction α of high-energy photons that cause photoionization depends upon the solid angle subtended by the disc and K star. The K star covers about 0.8 per cent of the sky as seen from the compact object, whereas the disc covers a fraction equal to the value of its vertical height divided by its radius H/R. The value of H/R is highly uncertain, but is of order 0.01 to 0.04. To be specific, we will assume that $\alpha = 0.02$. In the absence of an absolute flux calibration, we assume that during our observations the flux of A0620−00 at B was 60 per cent of the B flux measured by Haswell et al. (1993), on the basis that 17 per cent of the flux came from the disc in our data whereas ≈ 50 per cent of the flux in Haswell et al.'s data came from the disc. After correcting for 1.6 mag of extinction at B, we obtain a flux density at B of ≈ 0.2 mJy. Our upper limit on the equivalent width of He II 4686, $W_\lambda < 1$ Å, then becomes an upper limit on the rate of emission of ionizing photons N_P, given by

$$N_P < 2\,\frac{W_\lambda}{\lambda}\,\frac{f_\nu}{h}\,\frac{4\pi d^2}{\alpha\varepsilon}\,.$$

We have included a factor of 2 here, on the assumption that half of the He II 4686 photons are blocked by the disc.

Putting in the values discussed above, we find that, for our favoured mass of $M_1 = 3.7\,M_\odot$, $N_P < 9 \times 10^{41}$ photon s^{-1}; this limit changes with mass, since both M_1 and d are related through the orbital inclination. For a typical energy of an ionizing photon, 100 eV, we deduce that less than $\approx 10^{32}$ erg s^{-1} is emitted in the range 55 to 280 eV, corresponding to an accretion rate of 2×10^{12} g s^{-1} for a 6 per cent conversion of rest mass into energy for a non-rotating black hole.

This rate is sufficiently low to be a useful constraint: de Kool (1988) was only able to place a limit of 6×10^{14} g s^{-1} from X-ray upper limits, and Mineshige & Wheeler (1989) used a mass transfer rate of 10^{15} g s^{-1} to model the outbursts of A0620−00 (their model predicts a much lower accretion rate on to the compact object during quiescence, as we find here). However, our limit is only correct if the disc

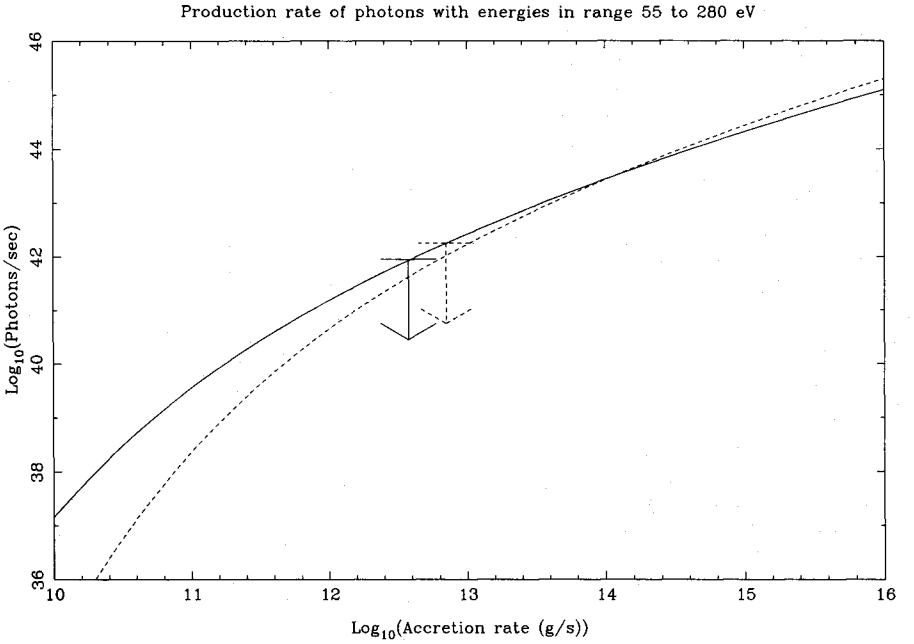

Figure 13. The rate of production of photons with energies between 55 and 280 eV from a steady-state, blackbody accretion disc around non-rotating black holes of masses 3.7 (solid line) and 10.4 $M_\odot$ (dashed) is plotted versus accretion rate. Upper limits derived from the absence of He II 4686 are plotted for each case.

emits a significant fraction of its luminosity in the 55–280 eV interval. As an approximate check, we computed the number of ionizing photons emitted by a steady-state disc as a function of mass transfer rate, assuming that the local spectrum was that of a blackbody with temperature defined by the standard distribution for a steady-state disc (Shakura & Sunyaev 1973). The results are plotted in Fig. 13 for two black hole masses, our favoured mass of $3.7\,M_\odot$ and a mass of $0.7/0.067 = 10.4\,M_\odot$ required to let the K star have a main-sequence mass. It can be seen from the plot that our approximate limit is not far out; we obtain a revised upper limit of 4×10^{12} g s^{-1} (or 7×10^{12} g s^{-1} for $M_1 = 10.4\,M_\odot$).

5 CONCLUSIONS

We have taken spectra of high spectral resolution and signal-to-noise ratio of the black hole candidate A0620−00. Spectra of the companion star are significantly broadened by rotation and, accounting for the geometry of the Roche lobe, we find a mass ratio of $q = M_2/M_1 = 0.067 \pm 0.01$ for A0620−00. Direct measurements of the emission-line radial velocities are roughly consistent with this value, but are distorted by the presence of emission from the gas stream and bright-spot. Doppler images show such emission extending from the red star to the bright-spot, and are very similar to those of quiescent dwarf novae. The position of the bright-spot and the separation of the emission-line peaks give a disc radius of $\approx 0.5\,R_{L1}$.

Our spectra give a precise measurement of the K star's radial velocity semi-amplitude $K_2 = 433 \pm 3$ km s^{-1}, somewhat lower than, but consistent with, previous measurements. Ellipsoidal variations reflected in the equivalent width of Hα are consistent in magnitude with the inclination deduced by Haswell et al. (1993), and this allows us to set 2σ limits on the masses of the component stars of $3.30 < M_1 < 4.24\,M_\odot$ and $0.15 < M_2 < 0.38\,M_\odot$. The mass of the compact object is higher than the maximum mass found for maximally rotating neutron stars with the stiffest equations of state proposed for nuclear material, but lower than the maximum possible mass if only causality constrains the equation of state.

At the time of our observations, the K star contributed the majority of the flux at both Hα (94 per cent) and Hβ (83 per cent). The K star shows Li I 6708 absorption with about half the equivalent width of the same line found in V404 Cyg, another black hole binary candidate. The dominance of the K star suggests that the disc is significantly dimmer than seen in the observations of Haswell et al. (1993).

We detected no He II 4686 in A0620−00, and so we were able to place an upper limit of 4×10^{12} g s^{-1} upon the accretion rate on to the black hole.

ACKNOWLEDGMENTS

We thank Phil Charles for his help in making these observations, and Tariq Shahbaz for helpful comments. The reduction and analysis were carried out on the Oxford node of the Starlink network. The WHT is operated on the island of La Palma by The Royal Greenwich Observatory in the Spanish Observatorio del Roque de Los Muchachos of the Instituto de Astrofísca de Canarias.

REFERENCES

Al-Naimiy H. M., 1978, Ap&SS, 53, 181
Anderson L., Shu F. H., 1977, ApJ, 214, 798
Barnes T. G., Evans D. S., 1976, MNRAS, 174, 489
Bochkarev N. G., Karitskaya E. A., Shakura N. I., 1979, SvA, 23, 8
Casares J., Charles P. A., Naylor T., 1992, Nat, 355, 614
de Kool M., 1988, ApJ, 334, 336
Eaton J. A., Poe C. H., 1984, Acta Astron., 34, 97
Elvis M., Page C. G., Pounds K. A., Ricketts M. J., Turner M. J. L., 1975, Nat, 257, 656
Friedman J. L., Ipser J. R., 1987, ApJ, 314, 594
Friedman J. L., Ipser J. R., Parker L., 1986, ApJ, 304, 115
Greenstein J. L., Kraft R. P., 1959, ApJ, 130, 99
Haswell C. A., Shafter A. W., 1990, ApJ, 359, L47
Haswell C. A., Robinson E. L., Horne K., Stiening R. F., Abbott T. M. C., 1993, ApJ, 411, 802
Horne K., 1986, PASP, 98, 609
Horne K., Saar S. H., 1991, ApJ, 374, L55
Hummer D. G., Storey P. J., 1987, MNRAS, 224, 801
Johnston H. M., Kulkarni S. R., 1990, in Mauche C. W., ed., Accretion Powered Compact Binaries. Cambridge Univ. Press, Cambridge, p. 17
Johnston H. M., Kulkarni S. R., Oke J. B., 1989, ApJ, 345, 492
King A. R., 1993, MNRAS, 260, L5
Lucy L. B., 1967, Z. Astrophys., 65, 89
McClintock J. E., Remillard R. A., 1986, ApJ, 308, 110 (MR)
McClintock J. E., Remillard R. A., 1989, BAAS, 21, 1206
McClintock J. E., Petro L. D., Remillard R. A., Ricker G. R., 1983, ApJ, 266, L27
Marsh T. R., 1988, MNRAS, 231, 1117
Marsh T. R., Horne K., 1988, MNRAS, 235, 269
Marsh T. R., Horne K., 1990, ApJ, 349, 593
Marsh T. R., Horne K., Schlegel E. M., Honeycutt R. K., Kaitchuck R. H., 1990, ApJ, 364, 637
Martin E. L., Rebolo R., Casares J., Charles P. A., 1992, Nat, 358, 129
Mineshige S., Wheeler J. C., 1989, ApJ, 343, 241
Moore C. E., 1972, A Multiplet Table of Astrophysical Interest. National Bureau of Standards, Washington, p. 66
Oke J. B., 1977, ApJ, 217, 181
Oke J. B., Gunn J. E., 1983, ApJ, 266, 713
Paczyński B., 1971, ARA&A, 9, 183
Paczyński B., 1977, ApJ, 216, 822
Patterson J., Raymond J. C., 1985, ApJ, 292, 550
Press W. H., Flannery B. P., Teukolsky S. A., Vetterling W. T., 1986, Numerical Recipes, The Art of Scientific Computing. Cambridge Univ. Press, Cambridge, ch. 10
Remillard R. A., McClintock J. E., Bailyn C. D., 1992, ApJ, 399, L145
Rieke G. H., Lebofsky M. J., 1985, ApJ, 288, 618
Robinson E. L., Zhang E.-H., 1986, ApJ, 305, 732
Russell H. N., 1945, ApJ, 102, 1
Sarna M. J., 1989, A&A, 224, 98
Schneider D. P., Young P. J., 1980, ApJ, 238, 946
Shafter A. W., 1983, ApJ, 267, 222
Shakura N. I., Sunyaev R. A., 1973, A&A, 24, 337
Tonry J., Davis M., 1979, AJ, 84, 1511
Wade R. A., Horne K., 1988, ApJ, 324, 411
Wade R. A., Rucinski S. M., 1985, A&AS, 60, 471
Wallerstein G., 1992, Nat, 356, 569
Wu C.-C., Aalders J. W. G., van Duinen R. J., Kester D., Wesselius P. R., 1976, A&A, 50, 445
Young P. J., Schneider D. P., 1980, ApJ, 238, 955

APPENDIX

In Section 3.1, we claimed that MR's cross-correlation analysis was affected by noise-induced correlation between their template and the spectra used to form it. In this appendix, we analyse this effect in order to determine when it could be important.

We define the cross-correlation C_i^n between the nth spectrum S^n and a template T as a function of the number of pixels offset between them, i, to be

$$C_i^n = \sum_j S_j^n T_{j-i},$$

where j numbers the pixels of the spectrum and end effects are neglected. For simplicity, assume that the template is formed from the average of the spectra after they have been shifted by integral numbers of pixels, $m(n)$, for spectrum n (determined by a circular orbit fit). If there are N spectra, the template is

$$T_i = \frac{1}{N} \sum_n S_{i+m(n)}^n,$$

and, avoiding repeated indices, the cross-correlation becomes

$$C_i^n = \sum_j S_j^n \frac{1}{N} \sum_k S_{j-i+m(k)}^k.$$

The spectra have noise on them, and the cross-terms generated from this have an expected value of zero for most terms, as the noise on different spectra is uncorrelated. However, this is not the case when $n = k$, for which the term is

$$\frac{1}{N} \sum_j N_j^n N_{j-i+m(k)}^n,$$

where N_i^n is the noise on the ith pixel of the nth spectrum. The expected value of this term is

$$\frac{1}{N} \sum_j V_j^n \delta_{j,j-i+m(k)},$$

where V^n is now the variance on the nth spectrum and we have introduced the Kronecker delta, which equals one if its indices are equal and zero otherwise. The indices are equal for $i = m(k)$, and therefore the cross-correlation of spectrum n has a spurious noise spike added, of strength $(\Sigma_j V_j^n)/N$, at whatever velocity shift was used in adding spectrum n into the template. For non-integral shifts, the same applies, although the spike will be smeared over a few pixels, depending upon the interpolation scheme used to shift the spectra.

The results of this analysis can be summarized as follows: if the spectra are noisy, whatever velocity is shifted out to form the template may come straight back as the maximum of the cross-correlation, and the strong peak may cause the estimated uncertainty to be spuriously low. A half-way point occurs when the spurious peak is the same height as the true peak, which is at most $\sum_j T_j^2$ if the spectra and template are identical and are scaled to have the same mean flux. At this point the peak height would still be overestimated by a factor of 2. Normalizing the continuum of our template spectra and subtracting 1, we find that $\sum_j T_j^2 \approx 3$ for the red arm (excluding Hα and Na I as these are corrupted by emission lines from the sky and target) and 30 for the blue arm, excluding Hβ. The blue arm gives a much larger value, as there are many more lines in the blue compared to the red. These values allow us to estimate the order of magnitude of the problem for MR's spectra.

MR's spectral region (4700 to 5600 Å) is closest to that of our blue data, and so we take $\sum T^2 = 30$. This must be corrected for the lower resolution of MR's data, 4 Å, and, assuming that the K-star lines are unresolved in each set of data, this gives $\sum T^2 = 30 \times 1.5/4 = 11$. From this, we can obtain a minimum signal-to-noise ratio to reach the breakpoint discussed above, although even this is distorted. Setting $(\sum V)/N = 11$ over 1000 pixels for a spectrum normalized to a unit continuum, we need a signal-to-noise ratio on the spectra of order $10/\sqrt{N}$, which is equivalent to a signal-to-noise ratio of 10 per pixel on the mean of all the spectra. Fig. 3 of MR shows the size of the uncertainty on the average spectrum averaged over five pixels, from which we estimate a signal-to-noise ratio of 8 per pixel.

This order-of-magnitude estimate indicates that the noise spike is probably the cause of the spuriously low uncertainty on MR's final fit. Our calculation is imprecise, since we do not have all the information to hand, and it does not include veiling by the disc, for example, or the change in signal-to-noise ratio over MR's spectra. Judging by the change in the estimated uncertainty from 60 to 8 km s^{-1} found by MR, the effect was about a factor of 3 stronger than our estimate suggests.

We finish by noting that the use of a shifted template is not, in principle, wrong, but that the standard error analysis is rendered invalid. An alternative approach may be to form a new template for each spectrum which includes all spectra except the one to be cross-correlated. This could introduce variable systematic effects, but generally the problem is only significant when statistical uncertainties dominate over systematics.